Coordination Chemistry Reviews, 70 (1986) 85–120
Elsevier Science Publishers B.V., Amsterdam – Printed in The Netherlands

SHARP LINE ELECTRONIC TRANSITIONS AND METAL–LIGAND ANGULAR GEOMETRY

PATRICK E. HOGGARD
Department of Chemistry, North Dakota State University, Fargo, ND 58105 (U.S.A.)
(Received 9 December 1985)

CONTENTS

A. INTRODUCTION

The thesis of this article is that full configuration interaction within the *d*-electron manifold should be used in ligand field calculations, and that when this is done, the effects of angular geometry on *d–d* electronic spectra become a worthwhile object of study. We will be particularly concerned with first-row d^3 complexes, though the methods are readily extended to other configurations. Lever's monograph [1] contains much of the necessary background as well as many of the matrix elements for the d^2 configuration.

The use of spin–orbit coupling in the Hamiltonian, of full configuration interaction, and of corrections to the ligand field Hamiltonian for coordination geometry (that is, for departures from 90° bond angles) generally lead

0010-8545/86/$12.60

to perturbations of tens to a few hundred cm^{-1} from the energies calculated without them. One may choose to neglect these for broad interconfigurational bands (e.g., $t_{2g}^3 \rightarrow t_{2g}^2 e_g$) with widths typically on the order of 2000 cm^{-1}, but they become very significant for the much sharper intraconfigurational transitions, with widths typically from 5 to 50 cm^{-1}, depending on the temperature and other conditions.

The need to consider the full d manifold is accepted for second and third-row transition metal complexes, for which spin–orbit coupling can be quite large. But it has been argued that the accuracy of the model itself is not great enough to render minor corrections significant for first-row complexes. This position cannot be totally refuted at present, but our preliminary answer is that while individual sharp line positions may not be predictable as accurately as they can be determined experimentally, the calculated splittings within groups of lines are much more significant. Sharp line splittings can be approached fairly successfully when full configuration interaction is used, and it is the splittings which are particularly affected by the ligand angular geometry.

One of the problems in modeling sharp line spectra is that there are not enough of them, that is, not enough spectra with reliably assigned sharp line transitions. Quite often the electronic transitions in question are sandwiched among a host of vibronic bands, rendering identification difficult. They are also readily obscured by more substantial broad bands.

For d^3 complexes, the sharp line transitions, i.e., those within the t_{2g}^3 configuration, are transitions from the $^4A_{2g}$ ground state to the ^2E_g, $^2T_{1g}$, and $^2T_{2g}$ excited states (all in O_h notation). Energetically these fall in two groups, the $^2E_g \rightarrow {}^2T_{2g}$ bands at higher energy than the others. In strict octahedral symmetry, in which the ^2T states are split by spin–orbit coupling, five sharp line transitions should be observable. For any lower symmetry, eight distinct nondegenerate transitions are expected (except for the ground state splitting). Thus, assuming they can be correctly identified, each observed line correspond to one calculated transition energy.

In contrast, the ^4T states in octahedral symmetry are each split by spin–orbit coupling into four components. One can only guess at the peak position of a group of closely overlapping bands. Since the calculated splittings are only about 10% of the band widths for first-row complexes (and may be smaller than that due to vibronic quenching effects [2]), spin–orbit coupling is generally ignored. However, under lower than octahedral symmetry the additional splitting arising from spin–orbit coupling can be significantly larger [3], and should not be dismissed.

An examination of the data for $[Cr(CN)_6]^{3-}$ illustrates rather starkly the problems to be faced. All five O^* doublets have been assigned as shown in Table 1. A fair fit is obtained by using a set of approximation equations due

TABLE 1

Electronic spectrum of $K_3[Cr(CN)_6]$ (in cm^{-1})

Experimental	Excited state	Calculated [d]	Calculated [e]	Calculated [f]	Calculated [g]
12,448 [a]	^2E_g	11,764	12,140	12,138	12,494
13,066 [a]	$^2T_{1g}(\Gamma_8)$	12,459	12,500	12,492	13,050
13,086 [a]	$^2T_{1g}(\Gamma_6)$	12,459	12,500	12,513	13,060
18,408 [b]	$^2T_{2g}(\Gamma_8)$	19,333	19,231	19,216	18,405
18,459 [b]	$^2T_{2g}(\Gamma_7)$	19,333	19,231	19,267	18,459
26,600 [c]	$^4T_{2g}$	26,600	26,600	26,602	26,601
32,500 [c]	$^4T_{1g}$	32,496	32,489	32,492	32,832

[a] Ref. 13, 20 K. [b] Ref. 47, 20 K. [c] Ref. 48, 300 K. [d] From eqn. (1); $\Delta = 26{,}600$; $B = 529$, $C = 2650$. [e] Full configuration interaction, no spin–orbit coupling; $\Delta = 26{,}600$, $B = 529$, $C = 2650$. [f] Full configuration interaction with spin–orbit coupling; $\Delta = 26{,}600$, $B = 529$, $C = 2650$, $\zeta = 124$. [g] Full configuration interaction with spin–orbit coupling and Trees correction; $\Delta = 26{,}600$, $B = 700$, $C = 1937$, $\zeta = 115$, α (Trees parameter) = 207.

to Jørgensen [4], in which spin–orbit coupling is neglected

$$
\begin{aligned}
&^4A_{2g} \rightarrow {}^2E_g \quad && \Delta E = 9B + 3C - 90B^2/\Delta \\
&^4A_{2g} \rightarrow {}^2T_{1g} \quad && \Delta E = 9B + 3C - 24B^2/\Delta \\
&^4A_{2g} \rightarrow {}^2T_{2g} \quad && \Delta E = 15B + 5C - 176B^2/\Delta \\
&^4A_{2g} \rightarrow {}^4T_{2g} \quad && \Delta E = \Delta \\
&^4A_{2g} \rightarrow {}^4T_{1g} \quad && \Delta E = 1.5\Delta + 7.5B - 0.5(\Delta^2 + 225B^2 - 18B\Delta)^{1/2}
\end{aligned}
\qquad (1)
$$

$\Delta = 10$ Dq is the octahedral ligand field splitting and B and C are Racah parameters.

Choosing Δ and B to fit the quartets, and C to give an approximate best fit to the doublets, the first column of calculated transition energies is generated. Note that the splitting between the lower set of doublets (^2E_g, $^2T_{1g}$) and the upper set ($^2T_{2g}$) is calculated to be much too large. Inclusion of full configuration interaction with these same parameters does improve this, though not nearly enough. If we now include spin–orbit coupling in order to generate a splitting of the ^2T states, we find that $\zeta = 124$ cm^{-1} reproduces both of these splittings very well, but does not otherwise improve the fit. For comparison, the free ion value of ζ for Cr^{3+} is 275 cm^{-1} [5].

Using sharp line spectral data to determine spin–orbit coupling constants for first-row transition metal complexes is a tenuous proposition. Firstly, neither the $^4A_{2g} \rightarrow {}^2E_g$ nor the $^4A_{2g} \rightarrow {}^2T_{1g}$ transition is affected to first or second order by the introduction of spin–orbit coupling, while the

$^4A_{2g} \rightarrow {}^2T_{2g}$ transition is subject to a second order perturbation [3]. Most of the effects we calculate are therefore of higher orders. Second, many apparently octahedral Cr(III) complexes exhibit ^2E_g splittings on the order of tens of wavenumbers [6–9], which may often be due to less than O_h symmetry in the crystal beyond the first coordination sphere. This raises the question of whether the $^2T_{1g}$ and $^2T_{2g}$ splitting may derive more from the crystal-induced low symmetry than from spin–orbit coupling. Certainly considerable uncertainty must attach to the calculated value of ζ in any system with substantial splitting due to low symmetry.

For $K_3[Cr(CN)_6]$, the ^2E_g splitting has been reported to be 48 cm^{-1} [9–12], which is quite large to explain as a low symmetry field from the crystal. Similar problems exist in the pentaammine series, the members of which tend to exhibit ^2E_g splittings on the order of 200 cm^{-1}, too large to be explained by the ligand field asymmetry [13,14]. Though there may be a reasonable explanation, for example, in terms of a ligand field potential from beyond the first coordination sphere, it should be recognized that splittings on the order of 100 cm^{-1} may occur which may not be explained by the model to be described here. Most of the splittings to be discussed will be larger than this, but it is interesting to note that, in spite of the unusual ^2E_g splitting in $K_3[Cr(CN)_6]$, the spin–orbit coupling constant derived from the $^2T_{1g}$ and $^2T_{2g}$ states is in fairly good agreement with the value of 90 cm^{-1} from recent magnetic measurements [15].

B. CALCULATIONS

The most common approach to d^n energy level calculations is to begin with a set of symmetry-adapted wavefunctions appropriate to the point group to which the molecule under consideration approximates. This may or may not be a complete set, but usually is chosen to be complete for the terms of the same spin multiplicity as the ground state. An alternative method, that of irreducible tensors [16], also makes full use of group theory to calculate the coupling coefficients, by which a reduced matrix element is to be multiplied to generate the energy eigenvalues without explicit reference to the eigenfunctions.

Both of these methods work best, as one would expect, for molecules of high symmetry. Each may continue to be used when the symmetry is only approximate, but they become increasingly unwieldy. It is furthermore not usually straightforward to include the extent of the deviation from the ideal symmetry, which is precisely what we are addressing in this article.

To take d^3 as an example, there are 120 atomic basis functions $(10!/n!(10-n)!)$. In O_h symmetry (that is, ignoring spin–orbit coupling),

this reduces to just 20 distinct energy levels, because of orbital and spin degeneracies. To include spin–orbit coupling requires the O^* group, and the number of distinct energy levels rises to 39. Because of Kramer's degeneracy, there are no more than 60 distinct levels for any molecule, and except in octahedral and tetrahedral symmetries there will be exactly 60, since in the remaining double groups there are no representations of degeneracy greater than two.

In tetragonal symmetry (D_4^*) the 60 energy levels are partitioned between two representations (30 each). Trigonal symmetry (D_3^*) is similar. In D_2^* all 60 energy levels belong to one representation. The advantages of symmetry adaptation of the wavefunction evaporate rapidly with descent in symmetry. Evaluating matrix elements over symmetry-adapted, multi-term wavefunctions consumes a great deal of computational time, and except for O^* and D_4^* systems, we prefer to ignore symmetry entirely and use the full 120 wavefunction atomic basis set. O^* and D_4^* have the advantage not only of substantial reduction in the size of the secular determinant, but also that the matrix elements can be chosen real. In the more general case this is not possible, again reducing the advantage of using adapted wavefunctions. The general d^3 secular determinant is thus 120×120, and complex hermitian.

(i) Basis functions

The strong field basis set is employed here. These are related to the ordinary atomic wavefunctions (designated by the m_l eigenvalues) according to Griffith [17]

$$
\begin{aligned}
(xy) &= \frac{-i}{\sqrt{2}}\{(2) - (-2)\} \\
(xz) &= \frac{-1}{\sqrt{2}}\{(1) - (-1)\} \\
(yz) &= \frac{i}{\sqrt{2}}\{(1) + (-1)\} \\
(x^2 - y^2) &= \frac{1}{\sqrt{2}}\{(2) + (-2)\} \\
(z^2) &= (0)
\end{aligned}
\tag{2}
$$

For computational purposes it is useful to maintain a standard order for multielectron wavefunctions. For the d wavefunctions with spin we have

used $(x\overset{+}{y})$, $(x\overset{+}{z})$, $(y\overset{+}{z})$, $(x^2 \overset{+}{-} y^2)$, $(\overset{+}{z}^2)$, $(x\bar{y})$, $(x\bar{z})$, $(y\bar{z})$, $(x^2 = y^2)$, $(\bar{z}^2)$.
The three-electron wavefunctions are thus

$$\phi_1 = (x\overset{+}{y})(x\overset{+}{z})(y\overset{+}{z})$$

$$\phi_2 = (x\overset{+}{y})(x\overset{+}{z})(x^2 \overset{+}{-} y^2)$$

$$\phi_3 = (x\overset{+}{y})(x\overset{+}{z})(\overset{+}{z}^2)$$

$$\phi_4 = (x\overset{+}{y})(x\overset{+}{z})(x\overset{+}{y})$$

$$\vdots$$

$$\phi_{119} = (x\bar{z})(x^2 = y^2)(\bar{z}^2)$$

$$\phi_{120} = (y\bar{z})(x^2 = y^2)(\bar{z}^2)$$

(ii) Interelectronic repulsion

Electrostatic repulsion is formulated as a two-electron operator, e^2/r_{12}. Thus the matrix elements between d^n wavefunctions are expressed as sums of two-electron elements. For d^3

$$\left\langle abc\left|\frac{e^2}{r_{12}}\right|abc\right\rangle = \left\langle ab\left|\frac{e^2}{r_{12}}\right|ab\right\rangle + \left\langle ac\left|\frac{e^2}{r_{12}}\right|ac\right\rangle + \left\langle bc\left|\frac{e^2}{r_{12}}\right|bc\right\rangle$$

$$\left\langle abc\left|\frac{e^2}{r_{12}}\right|abd\right\rangle = \left\langle bc\left|\frac{e^2}{r_{12}}\right|bd\right\rangle + \left\langle ac\left|\frac{e^2}{r_{12}}\right|ad\right\rangle$$

$$\left\langle abc\left|\frac{e^2}{r_{12}}\right|ade\right\rangle = \left\langle bc\left|\frac{e^2}{r_{12}}\right|de\right\rangle$$

The evaluation of interelectronic repulsion matrix elements on weak field atomic wavefunctions is discussed thoroughly in Lever [1] and elsewhere [18].

The matrix elements over the strong field wavefunctions are also derived in Lever [1]. For computational purposes it is perhaps easiest to express the interelectronic repulsion matrix element as the sum of two electrostatic terms, the second of which represents the interchange of one pair of electrons

$$\left\langle ab\left|\frac{e^2}{r}\right|cd\right\rangle = V(a, b, c, d) - V(a, b, d, c) \tag{3}$$

TABLE 2

Electrostatic terms. Wavefunctions are represented numerically: $xy(1)$, $xz(2)$, $yz(3)$, $x^2-y^2(4)$, $z^2(5)$. B and C are Racah parameters. The A terms are omitted

$V(1,1,1,1) = 4B+3C$	$V(2,2,4,5) = \sqrt{3}\,B$
$V(1,1,2,2) = 3B+C$	$V(2,2,5,5) = B+C$
$V(1,1,3,3) = 3B+C$	$V(2,3,2,3) = -2B+C$
$V(1,1,4,4) = C$	$V(2,4,2,4) = -2B+C$
$V(1,1,5,5) = 4B+C$	$V(2,4,2,5) = -2\sqrt{3}\,B$
$V(1,2,1,2) = -2B+C$	$V(2,5,2,5) = 2B+C$
$V(1,2,3,4) = 3B$	$V(3,3,3,3) = 4B+3C$
$V(1,2,3,5) = \sqrt{3}\,B$	$V(3,3,4,4) = 3B+C$
$V(1,2,5,3) = -2\sqrt{3}\,B$	$V(3,3,4,5) = -\sqrt{3}\,B$
$V(1,3,1,3) = -2B+C$	$V(3,3,5,5) = B+C$
$V(1,3,2,4) = -3B$	$V(3,4,3,4) = -2B+C$
$V(1,3,2,5) = \sqrt{3}\,B$	$V(3,4,3,5) = 2\sqrt{3}\,B$
$V(1,4,1,4) = 4B+C$	$V(3,5,3,5) = 2B+C$
$V(1,5,1,5) = -4B+C$	$V(4,4,4,4) = 4B+3C$
$V(2,2,2,2) = 4B+3C$	$V(4,4,5,5) = 4B+C$
$V(2,2,3,3) = 3B+C$	$V(4,5,4,5) = -4B+C$
$V(2,2,4,4) = 3B+C$	$V(5,5,5,5) = 4B+3C$

Seven additional terms are non-zero for each of the above terms. $V(a,b,c,d) = V(a,d,c,b) = V(b,a,d,c) = V(b,c,d,a) = V(c,b,a,d) = V(c,d,a,b) = V(d,a,b,c) = V(d,c,b,a)$.

The non-zero electrostatic terms are listed in Table 2. The general electrostatic term $V(a, b, c, d)$ is zero if either a and c or b and d have opposite spin.

(iii) Ligand field potential

The angular overlap model provides a convenient framework to incorporate ligand angular positions into the one-electron ligand field potential matrix, $\langle d_i | V_{LF} | d_j \rangle$. A particular ligand L will interact with each of the metal d orbitals (the strong field orbitals, defined for a predetermined set of cartesian axes), based on the σ and π overlap which can take place. The standard ligand position is taken to be on the z-axis. The σ-interaction with the d_{z^2} orbital raises the energy of the latter by the amount e_σ, presumed to be a constant for a given metal, ligand, and metal–ligand distance. The π-interaction with the d_{yz} orbital raises its energy by $e_{\pi s}$ (s stands for the sine dependence on the azimuthal angle ϕ of the yz function). Likewise, the energy of the d_{xz} orbital is raised by $e_{\pi c}$ (c for cosine). For some ligands the orientation of the π orbitals is immaterial, and we can drop the c and s labels, so that the d_{xz} and d_{yz} orbitals are each raised in energy by e_π. We

TABLE 3

Segment of transformation matrix for rotation of d orbitals so that new z-axis is in the direction (θ, ϕ), in spherical polar coordinates [22]

Old	$\mathbf{D}^{\sigma}$	
	$(z^2)'$	
xy	$(\sqrt{3}/4)(1-\cos 2\theta)\sin 2\phi$	
xz	$(\sqrt{3}/2)\sin 2\theta \cos \phi$	
yz	$(\sqrt{3}/2)\sin 2\theta \sin \phi$	
x^2-y^2	$(\sqrt{3}/4)(1-\cos 2\theta)\cos 2\phi$	
z^2	$(1/4)(1+3\cos 2\theta)$	
Old	$\mathbf{D}^{\pi c}$	$\mathbf{D}^{\pi s}$
	$(xz)' = \pi c$	$(yz)' = \pi s$
xy	$(1/2)\sin 2\theta \sin 2\phi$	$\sin \theta \cos 2\phi$
xz	$\cos 2\theta \cos \phi$	$-\cos \theta \sin \phi$
yz	$\cos 2\theta \sin \phi$	$\cos \theta \cos \phi$
x^2-y^2	$(1/2)\sin 2\theta \cos 2\phi$	$-\sin \theta \sin 2\phi$
z^2	$-(\sqrt{3}/2)\sin 2\theta$	0

will ignore the δ-interaction with the d_{xy} and $d_{x^2-y^2}$ here, but they are defined similarly, and are treated elsewhere [19]. Because of the different structure of the d_{z^2} orbital, a direct σ-interaction with one lobe of any of the other four d-orbitals would raise the energy of that orbital by $(3/4)e_{\sigma}$.

In the general case, for each coordinated ligand in turn the metal d-orbital set is rotated so that the d_{z^2} orbital points directly at the ligand. Any orthogonal transformation of the d orbitals yields equivalent results in energy calculations, but this particular one allows the factoring of σ and π contributions, and thus has some advantages to chemists. The transformation matrix for a general rotation of the d orbitals is not as well known as one might think, especially since it constitutes the general five-dimensional representation, $R^{(2)}$, of the three-dimensional rotation group, 0(3). Schmidtke [20] derived the transformation matrix from an induction formula of Wigner [21]. Schäffer later derived an equivalent representation by direct trigonometric methods [22].

Part of the transformation matrix is shown in Table 3, which gives the new d_{z^2}, d_{yz}, and d_{xz} orbitals as linear combinations of the original set, after alignment of the new d_{z^2} orbital to point toward a ligand with spherical polar coordinates (θ, ϕ) [23]. Additionally one might wish to rotate the d orbitals about the metal–ligand axis if there is a preferred π orientation, for which we refer to Schmidtke [20] or Schäffer [22]. The $\mathbf{D}^{\sigma}$ column represents the transformation for the new d_{z^2} orbital, with which the ligand will σ-bond. The $\mathbf{D}^{\pi s}$ and $\mathbf{D}^{\pi c}$ columns represent the transformation to the new d_{xz} and d_{yz} orbitals.

TABLE 4

$\mathbf{D}^{\sigma}$ and $\mathbf{D}^{\pi}$ arrays for a single ligand at an angular position $(\theta, \phi) = (60°, 0)$

Old orbitals	$\mathbf{D}^{\sigma}$	$\mathbf{D}^{\pi s}$	$\mathbf{D}^{\pi c}$
xy	0	0.866	0
xz	0.750	0	−0.500
yz	0	0.500	0
$x^2 - y^2$	0.650	0	0.433
z^2	−0.125	0	−0.750

To put this in terms of an example, consider a ligand in the xz plane, raised 30° from the x axis. In polar coordinates its angular position is (60°, 0). Table 4 shows the numerical results for the $\mathbf{D}^{\sigma}$, $\mathbf{D}^{\pi s}$, and $\mathbf{D}^{\pi c}$ arrays. The new (rotated) d_{z^2} orbital, whose energy is raised by e_{σ}, is a linear combination of the original d orbitals

$$(z^2)' = 0.750d_{xz} + 0.650d_{x^2-y^2} - 0.125d_{z^2}$$

Thus the ligand σ-interaction is spread around three of the original d orbitals. If off-diagonal terms were ignored, this would mean that each of these three d orbitals is raised in energy in proportion to the square of its coefficient: d_{xz} by $0.563e_{\sigma}$, $d_{x^2-y^2}$ by $0.422e_{\sigma}$, and d_{z^2} by $0.016e_{\sigma}$.

Likewise the new (rotated) d_{xz} and d_{yz} orbitals, each of which is raised in energy by e_{π} (assuming the π interaction is isotropic), are linear combinations of the original d orbitals.

$$(xz)' = -0.500d_{xz} + 0.433d_{x^2-y^2} - 0.750d_{z^2}$$

$$(yz)' = 0.866d_{xy} + 0.500d_{yz}$$

The energy of each (original) d orbital is raised in energy by a fraction of e_{π} corresponding to the square of the coefficients: d_{xz} by $0.250e_{\pi}$, $d_{x^2-y^2}$ by $0.187e_{\pi}$, d_{z^2} by $0.563e_{\pi}$, d_{xy} by $0.750e_{\pi}$, and d_{yz} by $0.250e_{\pi}$, all in addition to the σ-effects already discussed.

These are, however, just the diagonal terms. The original d orbitals are not (as the rotated orbitals are) eigenfunctions, and they will be mixed by the ligand field potential, which in our example is the potential from the ligand located at (60°, 0°). Looking again at Table 4, the rows represent the coefficients for the linear combination of rotated d orbitals corresponding to each original d orbital

$$d_{xy} = +0.866(yz)'$$

$$d_{xz} = 0.750(z^2)' - 0.500(xz)'$$

$$d_{x^2-y^2} = 0.650(z^2)' + 0.433(xz)' \text{ etc.}$$

The sum of the squares of the coefficients is not unity, and the rows are not orthogonal because the rotated $(xy)'$ and $(x^2-y^2)'$ orbitals are omitted. The off-diagonal elements (and the diagonal elements too, for that matter) are simply the row products. For example

$$\langle d_{xz} \mid V \mid d_{x^2-y^2} \rangle = (0.750)(0.650)\langle (z^2)' \mid V \mid (z^2)' \rangle + (0.500)(0.433)$$

$$\langle (xz)' \mid V \mid (xz)' \rangle = 0.488e_\sigma - 0.217e_\pi$$

In this way the entire $\langle d_i \mid V \mid d_j \rangle$ matrix is constructed

	xy	xz	yz	x^2-y^2	z^2
xy	$0.750e_\pi$	0	$0.433e_\pi$	0	0
xz		$0.563e_\sigma + 0.250e_\pi$	0	$0.488e_\sigma - 0.217e_\pi$	$-0.094e_\sigma + 0.375e_\pi$
xz			$0.250e_\pi$	0	0
x^2-y^2				$0.422e_\sigma + 0.187e_\pi$	$-0.081e_\sigma - 0.325e_\pi$
z^2					$0.016e_\sigma + 0.563e_\pi$

The eigenvalues of this matrix are, of course, just e_σ, e_π (twice), and 0, the ligand field-derived energies of the five rotated d orbitals themselves.

To complete the calculation of the $\langle d_i \mid V \mid d_j \rangle$ matrix, the procedure is repeated for the rest of the ligands in the coordination sphere and the results added. Thus, for example, $\langle d_{xy} \mid V \mid d_{xz} \rangle$ is the sum of the row products over all N ligands.

$$\langle d_{xy} \mid V \mid d_{xz} \rangle = \sum_{L=1}^{N} \left\{ D_1^{\sigma L} D_2^{\sigma L} e_{\sigma L} + D_1^{\pi sL} D_2^{\pi sL} e_{\pi sL} + D_1^{\pi cL} D_2^{\pi cL} e_{\pi cL} \right\}$$

$\mathbf{D}^{\sigma L}$, $\mathbf{D}^{\pi sL}$, and $\mathbf{D}^{\pi cL}$ are the transformation arrays of Table 3, different for each ligand L. The rows label the d orbitals (in the order xy, xz, yz, x^2-y^2, z^2). The general matrix element is

$$\langle d_i \mid V \mid d_j \rangle = \sum_{L=1}^{N} \left\{ D_i^{\sigma L} D_j^{\sigma L} e_{\sigma L} + D_i^{\pi sL} D_j^{\pi sL} e_{\pi sL} + D_i^{\pi cL} D_j^{\pi cL} e_{\pi cL} \right\} \tag{4}$$

Finally, the single electron matrix elements $\langle d_i \mid V \mid d_j \rangle$ are used to generate the ligand field part of the multielectron secular determinant. For 3-electron wavefunctions

$$\langle abc \mid V \mid abc \rangle = \langle a \mid V \mid a \rangle + \langle b \mid V \mid b \rangle + \langle c \mid V \mid c \rangle$$

$$\langle abc \mid V \mid abd \rangle = \langle c \mid V \mid d \rangle$$

$$\langle abc \mid V \mid ade \rangle = 0$$

(iv) Spin–orbit coupling

The spin–orbit coupling is evaluated most naturally on the weak field wavefunctions, $\mid m_l m_s \rangle$. The matrix elements of the one-electron operator

$\xi \mathbf{l} \cdot \mathbf{s}$ may, for d electrons, be written

$$\langle m_l m_s \,|\, \xi \mathbf{l} \cdot \mathbf{s} \,|\, m_l m_s \rangle = \zeta m_l m_s$$

$$\langle \overset{+}{m}_l \,|\, \xi \mathbf{l} \cdot \mathbf{s} \,|\, m_l \mp 1 \rangle = \tfrac{1}{2}\left[(2 - m_l)(3 + m_l)\right]^{1/2} \zeta$$

$$\langle \bar{m}_l \,|\, \xi \mathbf{l} \cdot \mathbf{s} \,|\, m_l \overset{+}{-} 1 \rangle = \tfrac{1}{2}\left[(2 + m_l)(3 - m_l)\right]^{1/2} \zeta$$

Transforming the weak field into the strong field basis yields the 10×10 hermitian matrix $\langle d_i \,|\, \xi \mathbf{l} \cdot \mathbf{s} \,|\, d_j \rangle$, whose elements are given elsewhere [3]. The matrix elements over multielectron wavefunctions are calculated as in the previous section.

(v) Optimization and error analysis

What has been presented to this point is a framework with which to calculate the d–d transition energies given the spherical interelectronic repulsion parameters, B and C, the spherical spin–orbit coupling parameter, ζ, the angular overlap parameters e_σ and e_π, for each different ligand, and the exact angular positions of each ligand. The secular determinant is complex hermitian. For odd electron systems each eigenvalue will be two-fold Kramers degenerate. For first row transition elements the spin state is usually fairly well defined, and may be determined for each eigenvalue by examination of the associated eigenvector. Some thought should be given to the diagonalization procedure, with respect to both speed and accuracy. We have on occasion noted spurious results from a Jacobi algorithm when two eigenvalues approached each other closely. A rapid and stable set of routines based on the Householder method is found in the EISPACK Guide [24].

The model may now be used, within the limits of its accuracy and applicability, in several ways. Given known angular positions, the remaining parameters may be refined. All of these parameters, but in particular the angular overlap parameters, which are intended to be widely transferable to different complexes, should be more reliable than if determined from the approximate geometry only. Alternatively, given a reasonable set of inter-electronic repulsion, spin–orbit coupling, and angular overlap parameters, the ligand angular positions may be treated as parameters and subjected to refinement. In this case some equivalencies would have to be established, or other assumptions made to reduce the total number of positional parameters from $2N$. Finally, in an intermediate situation, whichever parameters are either most reliably known in advance, or have the least effect on the transition energies to be fit, can be held constant, while the remainder, a mixture of positional and ligand field parameters, are refined.

The refinement takes the form of a fit of calculated to experimental spectroscopic data. Experimental data from sharp line intraconfigurational

transition are to be preferred, both because small shifts are more easily discernible and because they represent single transitions which can be compared one-to-one with calculated transition energies. By contrast, a broad band ${}^4A_{2g} \rightarrow {}^4T$ transition consists of six components, and the experimental peak position must, in general, be fit to an average of six different calculated values, not an entirely satisfactory undertaking.

In a least squares optimization, therefore, both for this reason and because the experimental precision is 10 to 100 times greater for the narrow lines, these must be more heavily weighted than the broad bands. The choice of a weighting scheme is critical. This is because the splittings among the narrow lines are more significant than the actual positions, since it is the splittings which are most sensitive to geometry. Typically we use a least squares formula of the type

$$f = \Sigma B^2 + 50\Sigma N^2 + 500\Sigma S^2 \tag{5}$$

where B is the difference between (average) calculated and experimental broad band energies, N is the same for narrow lines, and S is the difference between calculated and experimental splittings, selected from among the narrow lines. The coefficients are chosen to be inversely proportional to the approximate relative precision with which each quantity can be measured. Any optimization technique may be employed, but we have experienced more rapid and more reliable convergence with non-derivative methods, such as the Powell parallel subspace method [25,26]. The optimization must be repeated several times with different sets of starting parameters to verify that the global minimum has been found.

Error analysis is also essential following an optimization to assess the reliability of the refined parameters. There are at least two questions to be evaluated. One is how the experimental uncertainties are propagated through to uncertainties in the values of the refined parameters. These uncertainties are larger the smaller the effect of parameter changes on the calculated transition energies. The second question has to do with how a change in one parameter would affect the best fit values of the remaining ones. This can be assessed by the correlation coefficients. If any of these are too close to 1.0 for a given pair of parameters, then an arbitrary change in one of these can be compensated by a change in the other with a minimal alteration of the calculated energies.

In order to perform an error propagation calculation [27] a weight vector, $\mathbf{W}$, is required, which is the reciprocal of the variance (σ^2) for each observable.

$$\mathbf{W}_i = \frac{1}{\sigma^2(E_i)}$$

where E_i is an observed transition energy. Typical values for **W** might be 0.0025 and 1.0 for broad and narrow bands, respectively, representing experimental uncertainties of 20 and 1.0 cm^{-1} in peak positions. The observables are assumed to be uncorrelated themselves. The numerical partial derivative matrix A is also required,

$$A_{ij} = \frac{\partial E_i}{\partial x_j}$$

E_i is a calculated energy and x_j denotes the jth parameter. The matrix **B** is evaluated as

$$\mathbf{B} = (\mathbf{A}^T\mathbf{W}\mathbf{A})^{-1}$$

from which the propagated errors and correlation coefficients are calculated [28]

$$\sigma(x_i) = (B_{ii})^{1/2}$$
$$\rho(x_i, x_j) = \frac{B_{ij}}{\sigma(x_i)\sigma(x_j)} \tag{6}$$

When the correlation coefficients are too large it may be possible to uncouple parameters by choosing suitable combinations. For example, the Racah parameters B and C tend to be strongly correlated, whereas B and C/B are much less so. The eigenvectors of the correlation coefficient matrix provide some help in choosing appropriate linear combinations. The optimization routines generally converge more rapidly and more reliably with uncoupled parameters.

(vi) Corrections to interelectronic repulsion

Corrections involving additional parameters are always introduced reluctantly, but there is some point to this exercise in the case of interelectronic repulsion, since the sharp line splittings are scarcely affected by the corrections, while the relative locations of the broad with respect to the narrow bands sometimes can be greatly improved. A rigorous approach would abandon the spherical parameterization of electron–electron repulsion, but the number of distinct parameters even in an O_h symmetry-based scheme [17] is too large to be practical.

The Trees correction [28] was proposed as an additional term of the form $\alpha L(L+1)$ to fit free ion spectra. The physical basis for the inclusion of this term remains obscure, although its form, as the eigenvalues of the operator

$\mathbf{L}^2$, suggests some kind of orbit–orbit interaction [29]. The $\mathbf{L}^2$ operator may be expressed as [30]

$$\mathbf{L}^2 = \left(\sum_i^n \mathbf{l}_i\right) \cdot \left(\sum_i^n \mathbf{l}_i\right) = \sum_i \mathbf{l}_i^2 + 2\sum_{i<j} \mathbf{l}_i \cdot \mathbf{l}_j$$

$$= \sum_i \mathbf{l}_i^2 + 2\sum_{i<j} \ell_{iz}\ell_{jz} + \sum_{i<j} (\ell_{i+}\ell_{j-} + \ell_{i-}\ell_{j+})$$

where ℓ_+ and ℓ_- are the raising and lowering operators. The matrix elements are then readily evaluated on the weak field wavefunctions

$$\mathbf{L}^2 \ |m_1, m_2, \ldots m_n\rangle = \left(6n + 2\sum_{i<j}^{n} m_i m_j\right) \ |m_1, m_2, \ldots m_n\rangle$$

$$+ \sum_i^n \{(3 + m_i)(2 - m_i)(3 - m_j)(2 + m_j)\}$$

$$\times |m_1, ..m_i + 1, \ldots m_j - 1, \ldots m_n\rangle \qquad (7)$$

Likewise, the matrix elements over the strong field wavefunctions are evaluated by expressing them as linear combinations of weak field functions (eqn. 2).

Several investigators have suggested that a Trees correction be routinely included [31–34], a step which would have consequences in the accepted values for B and C. A value of 70 cm^{-1} for α is frequently used [35], as suggested by free ion spectra of Cr(III) and other ions [36]. To the extent that orbit–orbit interaction is responsible for this effect, one would expect the magnitude to be altered. Orbital angular momentum is often quenched in complexes, so that the Trees Hamiltonian term might be formulated as $k^2\alpha\mathbf{L}^2$, where α is the free ion value and k is the orbital reduction factor, which can often be determined from magnetic experiments. In some optimizations, however, we have seen convergence to values larger than 70 cm^{-1} (see below).

A second idea for the correction of the interelectronic repulsion part of the calculation has been called differential orbital expansion by Jørgensen. Working from the hypothesis that the reduction in complexes of B and C from their free ion values is due to expansion of the metal d orbitals through overlap with the ligands, it would follow that in 6-coordinate complexes the $d_{x^2-y^2}$ and d_{z^2} orbitals would be subject to greater expansion than the d_{xy}, d_{xz}, and d_{yz} orbitals, which overlap less extensively. Experimentally this can be confirmed by determining B separately for $t_{2g} \rightarrow t_{2g}$ and $t_{2g} \rightarrow e_g$ transitions; B turns out invariably to be smaller for the latter, presumably due to the greater expansion of the e_g orbitals [37].

Mathematically this can be modeled in the strong field basis by adding a reduction factor to repulsion integrals when e_g orbitals are involved [38]

$$\left\langle ab\left|\frac{e^2}{r_{12}}\right|cd\right\rangle = \epsilon^n\left\langle ab\left|\frac{e^2}{r_{12}}\right|cd\right\rangle^0$$

where n is the number of e_g wavefunctions (0 to 4) appearing in the integral.

There is considerable debate over how best to correct the treatment of interelectronic repulsion within the ligand field model [33]. This debate is worthwhile, since the number of distinct repulsion integrals, unrelated by symmetry, is quite large in non-spherical environments. The Trees correction and differential orbital expansion are quite different in origin, and they can, of course, both be applied. This is not unreasonable because the sharp line splitting will be scarcely affected by either. However, even aside from considerations of simplicity and the problems of overparameterization, it would be very useful to settle on a standard approach so that sets of parameters can be usefully compared. At one time there was a de facto standard, in which C was set equal to $4B$, and B calculated by analysis of spin-allowed transitions. Despite its arbitrariness, it was a very useful construct. At present we lack a standard approach suitable for inclusion of sharp line transitions with appropriate precision. So the debate as to whether a Trees correction is more suitable than the invocation of differential orbital expansion is important, and it should be remembered that the goal is to position accurately the $t_{2g} \rightarrow t_{2g}$ and $t_{2g} \rightarrow e_g$ transitions. From our own trials on d^3 complexes, we have found a Trees correction generally more effective on first-row complexes, but differential orbital expansion appears to be useful for the second and third row.

(vii) Pi anisotropy

The angular overlap framework for construction of the $\langle d_i \mid V_{LF} \mid d_j \rangle$ matrix in Section C allows in principle for anisotropic ligand–metal π interactions by permitting $e_{\pi s}$ and $e_{\pi c}$ to adopt different values, an ineffective means to this end because of the difficulty in partitioning properly between $e_{\pi s}$ and $e_{\pi c}$. Thus the angular overlap arrays $\mathbf{D}^{\pi s}$ and $\mathbf{D}^{\pi c}$ of Table 3 should really only be used for ligands presenting a cylindrically symmetrical set of π orbitals to the metal, such as NH_3 (lacking π orbitals altogether), halides, CN^-, and probably NCS^-.

Other ligands usually present one π orbital, the orientation of which affects the metal d orbital energies significantly. The π orbital of a coordinated water molecule, for example, may be presumed to be perpendicular to the M–O and the O–H bonds. This is treated by including a third angle, ψ,

in the $\mathbf{D}^{\pi s}$ and $\mathbf{D}^{\pi c}$ arrays to allow rotation of the coordinate system to place the ligand in any convenient orientation. The reader is referred to Schäffer's article for the full $\mathbf{D}^{\pi s}$ and $\mathbf{D}^{\pi c}$ arrays [22].

The angle ψ must be determined separately for each ligand, which is not a trivial task, because each ligand begins in a particular θ- and ϕ-dependent orientation following rotation of the coordinate system to point the z axis in the direction of the ligand. However, given the ligand angular position (θ, ϕ) and a vector $(\mathbf{a}, \mathbf{b}, \mathbf{c})$ representing a bond vector to which the π orbital should be perpendicular (in addition to the metal–ligand bond), the angle ψ may be calculated which will align the (transformed) y axis parallel to the ligand π orbital

$$\cos^2\psi = \frac{(a\cos\phi\cos\theta + b\sin\phi\cos\theta - c\sin\theta)^2}{(a\cos\phi\cos\theta + b\sin\phi\cos\theta - c\sin\theta)^2 + (a\sin\phi - b\cos\phi)^2} \tag{8}$$

Caution must be used in selecting the proper sign of ψ. Using this value of ψ in the $\mathbf{D}^{\pi s}$ and $\mathbf{D}^{\pi c}$ arrays [23], $e_{\pi c} = 0$ and the π-interaction of the ligand is expressed entirely through $e_{\pi s}$.

Does π-anisotropy make a difference? Indeed it does. Figures 1 and 2 show two sets of sample calculations for a *cis*-$[Cr(IDA)_2]^-$ complex

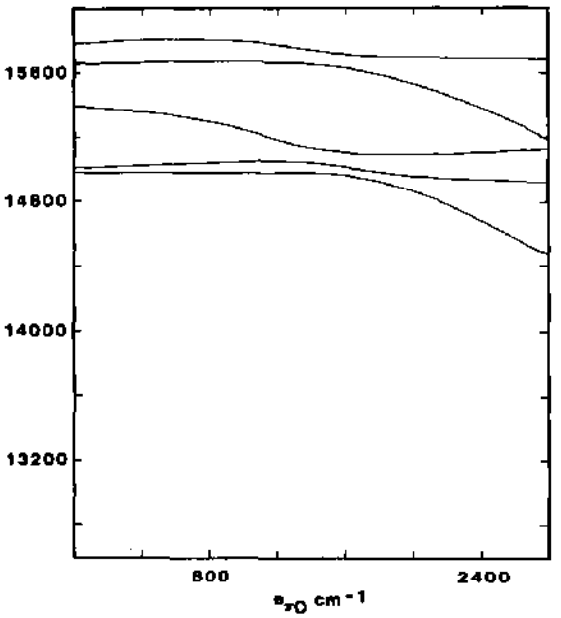

Fig. 1. Calculated (^2E_g, $^2T_{1g}$) transition energies for $K[Cr(IDA)_2]$ as a function of an isotropic $e_{\pi O}$, $e_{\sigma N} = 7000$, $e_{\sigma O} = \frac{1}{3}(19{,}500 - 4e_{\pi O})$, $B = 650$, $C = 2650$, $\zeta = 250$, $\alpha = 0$. The last four values are used in all subsequent energy plots.

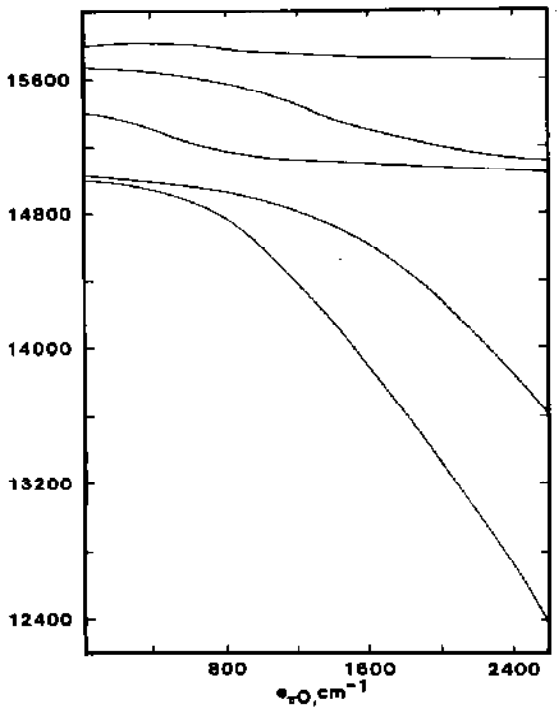

Fig. 2. Calculated (^2E_g, $^2T_{1g}$) transition energies for K[Cr(IDA)$_2$] as a function of an anisotropic $e_{\pi O}$. $e_{\sigma N} = 7000$, $e_{\sigma O} = \frac{1}{3}(19{,}500 - 2e_{\pi O})$.

(H_2IDA = iminodiacetic acid) using the actual atom positions from an X-ray structure determination on the potassium salt [39]. Although carboxylate oxygens have two electron pairs after forming a sigma bond to the metal, the approximately 120° M–O–C angles [39] indicate strongly that the π-donation is limited to one of these pairs, with the other a non-bonding pair at the third apex of a triangle around the oxygen.

In Figs. 1 and 2 the five ^2E_g and $^2T_{1g}$ components are plotted against $e_{\pi O}$, varying $e_{\sigma O}$ at the same time to keep the quartet energies approximately constant. In Fig. 1 both electron pairs were assumed to interact with π symmetry simultaneously, and with no dependence on orientation. In Fig. 2 $e_{\pi C}$ was set equal to zero and the angle ψ was determined from the O–C bond vectors and eqn. 8.

Although Figs. 1 and 2 demonstrate primarily that the introduction of π-anisotropy markedly alters energy level calculations, especially of the sharp lines, comparison with experimental results (see below) leaves no doubt about the inadequacy of the isotropic approximation. For carboxylate and other ligands with similar geometric constraints, an anisotropic π interaction ought to be employed routinely and exclusively. This does, however, create the knotty problem of fixing the orientation of the π orbital when structural information is unavailable.

(viii) Redundancy

The question of redundancy arises in ligand field treatments involving the angular overlap model. In an O_h complex with a linearly ligating group, the single orbital energy difference, represented by Dq, is replaced by e_σ and e_π, related by $10\ Dq = 3e_\sigma - 4e_\pi$. Similarly, in a D_{4h} MA_4B_2 complex the three orbital energy differences, represented by Dq, Ds, and Dt, are replaced by four AOM parameters. The redundancy of one must be resolved by assigning one AOM parameter arbitrarily, generally with reference to e_π of a saturated amine being zero.

In a D_{2h} $MA_2B_2C_2$ complex all five diagonal d orbital energies are distinct (i.e., there are four energy differences), and there is a non-zero off-diagonal matrix element, $\langle x^2 - y^2 \mid V \mid z^2 \rangle$, for a total of five parameters, while the AOM set of six is still redundant by one. $3e_\sigma - 4e_\pi$ for a linearly ligating ligand can still be set equal to $10\ Dq$ for a possibly hypothetical octahedral complex.

For a low symmetry molecule there are 15 global ligand field parameters, 5 diagonal and 10 off-diagonal matrix elements. These are highly redundant, since this set can be reduced to the five d orbital eigenvalues plus three Euler angles necessary to rotate the d orbitals into the orientations defined by the eigenvectors. These rotational angles cannot be determined from the geometry alone in the global model, and so must be included in the parameter set. Considering only energy differences, there are at most seven independent parameters in the global model, though there is no straightforward way to define them except by diagonalization of the $\langle d_i \mid V \mid d_j \rangle$ matrix. It is thus possible for an AOM parameter set to be redundant by more than one dimension.

This situation is drastically altered when π-anisotropy is considered. The effective symmetry of the metal ion is lowered, perhaps extensively. Take for example a $[M(H_2O)_6]^{n+}$ complex with an O_h MO_6 group. Even with an optimally symmetric orientation of oxygen π orbitals, one additional, off-diagonal matrix element is introduced [22], and in other orientations still more. $[Cr(ox)_3]^{3-}$, considering its actual geometry and the oxygen π orientations, has no symmetry, even approximately. Although very roughly one could say that $10\ Dq = 3e_\sigma - 2e_\pi$, in fact Dq is not defined, since even in the most symmetric O_h approximation, more than one $t_{2g} - e_g$ energy difference is involved. The AOM set is no longer redundant. In fact, since the geometry may be entered explicitly, the angular overlap model represents with just two parameters what is a seven-dimensional problem in the global model. There is considerable leeway in other complexes to introduce the geometry parametrically without exceeding the actual dimensionality of the ligand field portion of the problem.

C. SOME SPECIAL GEOMETRIES

Having decided on a representation for the interelectronic repulsion and spin–orbit coupling parts, the remaining geometry-dependent task centers on constructing the $\langle d_i \mid V_{LF} \mid d_j \rangle$ matrix. Given structural information, this is straightforward, but one of the more interesting applications is to develop the ligand potential matrix as a function of the independent angles for certain geometries.

Tris(bidentate) $M(A–A)_3$ complexes

Two independent angles are involved which we represent in terms of deviations from orthoaxial ligand positions, as shown in Fig. 3. The angle α gives the contraction (or expansion, if negative) from a 90° bond angle. The traditional chelate bite angle is thus $90° - 2\alpha$. The angle β describes the rotation of the A–A axis out of the cartesian plane. As suggested by Schäffer [40], we define β as positive when, sighting from the outside towards the central metal, the ligator on the left is displaced upwards and that on the right downwards. The more usual twist angle, that between the two triangles perpendicular to the C_3 axis, is related to both α and β in a rather complicated fashion. To emphasize that α and β are defined as angular displacements relative to a cartesian frame, we will refer to them as the cartesian bite and twist angles, respectively.

For a complex (a Δ isomer) numbered as

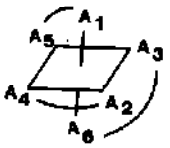

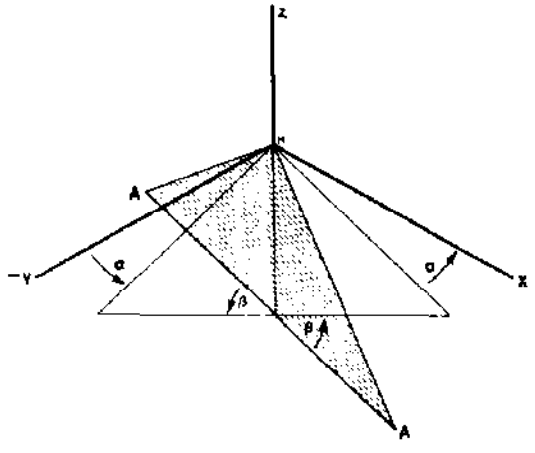

Fig. 3. Cartesian bite (α) and twist (β) angles for an M(A–A) unit. β is positive in the orientation shown.

TABLE 5

Polar coordinates for a Δ-M(A–A)$_3$ complex

	θ	ϕ
A_1	$\cos^{-1}(\cos\sigma\cos\rho)$	$180+\tan^{-1}(\frac{\tan\rho}{\sin\sigma})$
A_2	$90+\rho$	$-\sigma$
A_3	$\cos^{-1}(-\sin\sigma\cos\rho)$	$180+\tan^{-1}(-\frac{\cos\sigma}{\tan\rho})$
A_4	$90-\rho$	$270+\sigma$
A_5	$\cos^{-1}(\sin\sigma\cos\rho)$	$180+\tan^{-1}(-\frac{\tan\rho}{\cos\sigma})$
A_6	$\cos^{-1}(-\cos\sigma\cos\rho)$	$\tan^{-1}(\frac{\sin\sigma}{\tan\rho})$

$\rho = \sin^{-1}\{\frac{1}{\sqrt{2}}(\cos\alpha-\sin\alpha)\sin\beta\}$. $\sigma = \tan^{-1}\{\frac{(\cos\alpha+\sin\alpha)-(\cos\alpha-\sin\alpha)\cos\beta}{(\cos\alpha+\sin\alpha)+(\cos\alpha-\sin\alpha)\cos\beta}\}$.

this leads to polar coordinates $(\theta, \phi) = (90-\rho, 270+\sigma)$ for ligand A_4 (ρ and σ are defined in Table 5), and since A_2 will suffer the same angular displacement, ρ, below the xy plane, coordinates $(90+\rho, -\sigma)$ for A_2. In cartesian coordinates these are

A_4: $(\sin\sigma\cos\rho, -\cos\sigma\cos\rho, \sin\rho)$

A_2: $(\cos\sigma\cos\rho, -\sin\sigma\cos\rho, -\sin\rho)$

Rotation about the (1, 1, 1) C_3 axis results in a cyclic permutation of coordinates. Table 5 lists polar coordinates for each ligand.

The V_{LF} matrix can be constructed as described in Section B. The angular coordinates of Table 5 are inserted into the **D** arrays of Table 3, and the

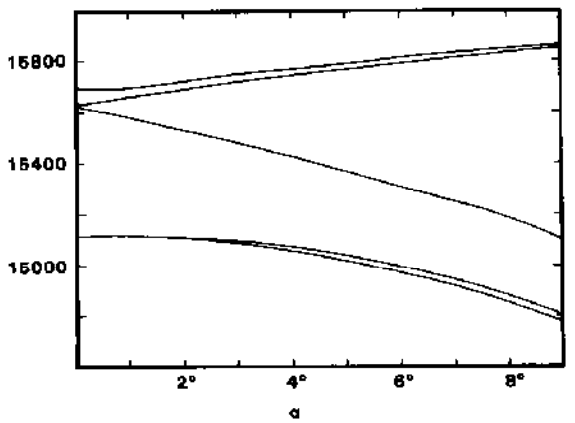

Fig. 4. Calculated (^2E_g, $^2T_{1g}$) transition energies for a $[Cr(en)_3]^{3+}$ complex as a function of the cartesian bite angle. $e_{\sigma N} = 7000$, $\beta = 0$.

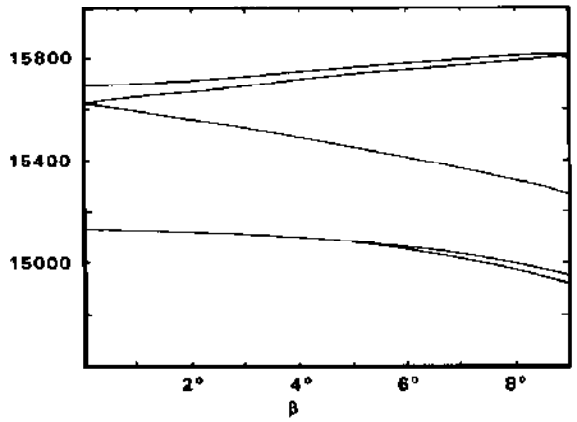

Fig. 5. Calcualted (^2E_g, $^2T_{1g}$) transition energies for a $[Cr(en)_3]^{3+}$ complex as a function of the cartesian twist angle. $e_{\sigma N} = 7000$, $\alpha = 0$.

$\langle d_i \mid V_{LF} \mid d_j \rangle$ matrix elements are calculated with eqn. 4. Thus with appropriate values for e_σ, e_π, ζ, and the interelectronic repulsion parameters, the effects of changes in α and β on transition energies can be modeled. Figures 4 and 5 show some results of calculations for a $Cr(A{-}A)_3$ complex with no π-interaction on the transition energies to the five components of the octahedral ^2E_g and $^2T_{1g}$ states. The bite and twist distortions have similar effects on the splittings, most obviously the movement of one component away from the $^2T_{1g}$ group towards the ^2E_g with increasing distortion of either type.

Triazacyclononane complexes

The coordination of two [9]ane-1,4,7-N_3 ligands can also be represented in terms of a bite and a twist angle which are zero when the CrN_6 skeleton is octahedral. For the complex

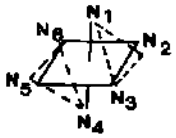

each ligand of the $N_1N_2N_3$ triangle is displaced by an angle α from the coordinate axis towards the molecular C_3 axis, followed by a twist, by an angle β, defined as positive for a clockwise motion of the triangle, viewed from the outside, with a corresponding twist in the opposite direction by the $N_4N_5N_6$ triangle. The cartesian bite angle, α, can be expressed in terms of the N_1CrN_2 bond angle θ

$$\alpha = \cos^{-1}\left\{\tfrac{1}{3}(1 + 2\cos\theta)^{1/2} + \tfrac{2}{3}(1 - \cos\theta)^{1/2}\right\}$$

$$\theta = \cos^{-1}\left\{\tfrac{1}{2}\sin^2\alpha + \sqrt{2}\sin\alpha\cos\alpha\right\}$$

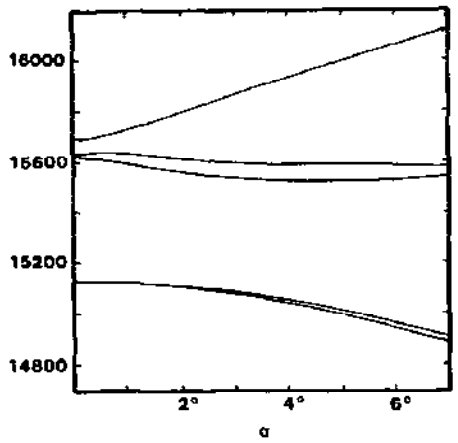

Fig. 6. Calculated (^2E_g, $^2T_{1g}$) transition energies for a $[Cr(\overline{N-N-N})_2]^{3+}$ complex as a function of the trigonal cartesian bite angle. $e_{\sigma N} = 7000$, $\beta = 0$.

The cartesian coordinates of atoms N_1 and N_4 are then

$$N_1: \begin{pmatrix} \frac{1}{\sqrt{2}} \sin\alpha(\cos\beta + \sqrt{3}\sin\beta + 2) + \cos\alpha(-\cos\beta - \sqrt{3}\sin\beta + 1) \\ \frac{1}{\sqrt{2}} \sin\alpha(\cos\beta - \sqrt{3}\sin\beta + 2) + \cos\alpha(-\cos\beta + \sqrt{3}\sin\beta + 1) \\ \frac{1}{\sqrt{2}} \sin\alpha(-2\cos\beta + 2) + \cos\alpha(2\cos\beta + 1) \end{pmatrix}$$

$$N_4: \begin{pmatrix} \frac{1}{\sqrt{2}} \sin\alpha(-\cos\beta + \sqrt{3}\sin\beta - 2) + \cos\alpha(\cos\beta - \sqrt{3}\sin\beta - 1) \\ \frac{1}{\sqrt{2}} \sin\alpha(-\cos\beta - \sqrt{3}\sin\beta - 2) + \cos\alpha(\cos\beta + \sqrt{3}\sin\beta - 1) \\ \frac{1}{\sqrt{2}} \sin\alpha(2\cos\beta - 2) + \cos\alpha(-2\cos\beta - 1) \end{pmatrix}$$

The cartesian coordinates of the remaining atoms are obtained by cyclic permutation. The spherical polar coordinates derived from these are then used to set up the $\langle d_i | V_{LF} | d_j \rangle$ matrix. Figure 6 shows the calculated effects of changes in α on the Cr(III) ^2E_g and $^2T_{1g}$ lines. Changes in β lead to smaller effects. A 2-2-1 splitting pattern would appear to be characteristic of this geometry for moderate values of α and β.

CrN_5A complexes

It might be imagined that coordinating five bulky groups, such as alkylamines, would have the effect of pushing the four groups in the xy plane

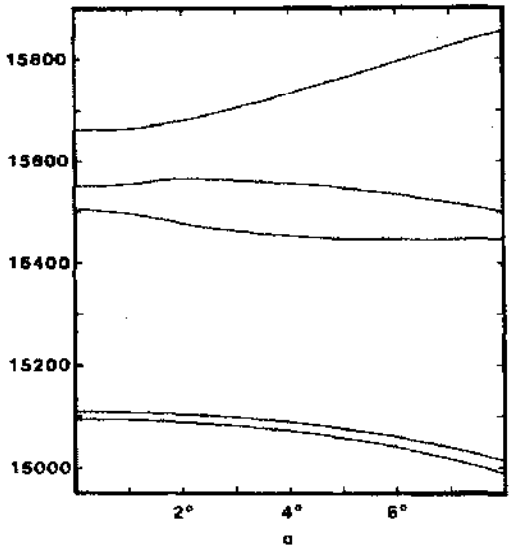

Fig. 7. Calculated (^2E_g, $^2T_{1g}$) transition energies for a trigonally distorted CrN_5Cl chromophore as a function of the cartesian bite angle. $e_{\sigma N} = 7000$, $e_{\sigma Cl} = 6400$, $e_{\pi Cl} = 900$.

out of that plane and towards the smaller A ligand. Crystal structures of $[M(EtNH_2)_5Cl]^{2+}$ salts (M = Co, Cr), however, expose a much more complex pattern of distortion [41], but one that can be approximated to some extent as a movement of the chloride and two amines towards each other, resembling somewhat the triazacyclononane geometry. In this approximation we have the following polar coordinates for the coordinating atoms

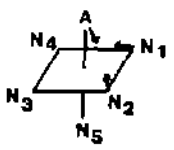

$$N_1\colon \left\{\cos^{-1}\left(\sin\alpha/\sqrt{2}\right), \tan^{-1}\left(\sqrt{2}\ \cot\alpha\right)\right\}$$

$$N_2\colon \left\{\cos^{-1}\left(\sin\alpha/\sqrt{2}\right), \tan^{-1}\left(\tan\alpha/\sqrt{2}\right)\right\}$$

$$N_3\colon (90°, 270°)\ N_4\colon (90°, 180°)\ N_5\colon (180°, 0)\ A\colon (\alpha, 45°)$$

It should be noted that with little geometric distortion, a ^2E_g splitting of the order of 200 cm^{-1} is observed in $[Cr(NH_3)_5X]$ complexes [13,14], which this model does not explain. Taken qualitatively, however, Fig. 7 illustrates the expected behavior of the (^2E_g, $^2T_{1g}$) transition energies as this type of distortion is introduced.

D. SOME EXPERIMENTAL RESULTS

Reliable sharp line electronic spectral data are sparse. Minimally for d^3 complexes such data ought to include the energies of the ^2E_g and $^2T_{1g}$ components, as well as what may be discerned of the quartets. Part of the reason for the scarcity of experimental data is that an unambiguous assign-

ment of electronic lines can be very difficult from a spectrum awash with multiple series of vibronic sidebands.

(i) Octahedral complexes

Full configuration calculations have been performed on octahedral complexes for some time [42–46]. The sharp line splittings are due, within the assumption of a strict O_h environment, entirely to spin–orbit coupling, although for first-row complexes a low symmetry field from the crystalline environment beyond the first coordination sphere may also be important. Octahedral complexes provide good test cases for assessing that portion of the model not dependent on angular geometry, and we will pay particular attention to the usefulness of corrections to the interelectronic repulsion term.

The last column of Table 1 presents the results of an optimization on $[Cr(CN)_6]^{3-}$, using eqn. 5 as the function to be minimized. Fitting the positions of the quartets and the ^2E and $^2T_1$ groups can be done reasonably well, but only at the cost of using a very large Trees correction, with $\alpha \sim 200$ cm^{-1}. This, of course, makes the values of B and C difficult to compare with complexes treated without a Trees correction. The doublet splittings are also not fit perfectly, although the value of the spin–orbit coupling parameter is about the same as that determined from a fit directed at the splittings.

TABLE 6

Calculated transition energies for d^3 complexes following optimization (in cm^{-1}; experimental values in parentheses)

Excited state	Cs_2ReF_6 [a]	$Cs_2NaMoCl_6$ [b]	IrF_6 [c]	$K_3[Cr(NCS)_6]$ [d]
^2E_g	8975 (9080)	9099 (9239)	6260 (6260)	12873 (12862)
$^2T_{1g}(\Gamma_8)$	10160 (10130)	9442 (9387)	8330 (8330)	13578 (13569)
$^2T_{1g}(\Gamma_6)$	11183 (11160)	9617 (9556)	8860 (8860)	13620 (13619)
$^2T_{2g}(\Gamma_7)$	17408 (17390)	14639 (14667)	12330 (12330)	18467
$^2T_{2g}(\Gamma_8)$	18681 (18670)	14468 (14412)	15160 (15160)	18366
$^4T_{2g}$	32805 (32800)	19200 (19200)	40551	17696 (17700)
$^4T_{1g}$	42092	24484 (23900)		23913 (23800)
$^4T_{1g}$				31167 (32400)
$^2T_{1g}$ splitting	1024 (1030)	175 (169)	530 (530)	43 (50)
$^2T_{2g}$ splitting	1273 (1280)	171 (255)	2830 (2830)	101

[a] Doublets from ref. 49, 20 K; quartets from Ref. 50, 295 K. $B = 683$, $C = 1495$, $\zeta = 3054$, $\alpha = -26$. [b] Doublets from ref. 51, 10 K; quartets from Ref. 6, 295 K, $B = 487$, $C = 1794$, $\zeta = 597$, $\alpha = 2$. [c] Doublets from ref. 52, vapor phase. $B = 633$, $C = 2398$, $\zeta = 3331$, $\alpha = 150$. [d] Doublets from ref. 53, 80 K; quartets from ref. 6, 295 K, $B = 741$, $C = 2039$, $\zeta = 285$, $\alpha = 218$.

Without a Trees correction it is impossible to fit the doublet groups and the quartets simultaneously, and applying a correction for differential orbital expansion is, as it turns out, little help. That the Trees correction is found to be so large, in comparison with a free ion value of 50–100 cm^{-1} [36], could well be due to the problems of using broad band data. Although broad band peak positions do represent vertical transitions, upon which the ligand field model is supposed to be predicated, the temperature dependence of these peak positions is quite different from that for the sharp lines, which is one indication of the difficulty in treating broad bands and sharp lines together.

In Table 6 are presented results from similar optimizations on some second and third-row complexes, as well as on $[Cr(NCS)_6]^{3-}$. As with $[Cr(CN)_6]^{3-}$, the data are taken from more than one source, the broad bands from room temperature absorption spectra and the sharp electronic lines from low temperature absorption or excitation. No differential orbital expansion was included, and (except for IrF_6) Δ was fixed to fit the $^4T_{2g}$ band, rather than optimized over all transitions.

The fits are generally good, both as to band positions and, more importantly, splittings, with the exception of $[MoCl_6]^{3-}$. Although for this complex the Trees correction proved of little use, the fit can be improved by employing a differential orbital expansion factor ϵ of about 0.75, but still not to the degree of fit shown by the others.

(ii) Chromium(III) complexes

Sufficient sharp line data are available for a few Cr(III) chelate complexes to examine the implications for metal–ligand geometry. Table 7 presents assignments for the five components of the ^2E_g and $^2T_{1g}$ states, which are, except as indicated, those of the authors referenced. In many cases these assignments are uncertain or incomplete. We have therefore not optimized parameters nor used a Trees correction.

$[Cr(en)_3]^{3+}$ is an obvious starting point, but presents some problems. Figures 4 and 5 illustrate the calculated dependence of the sharp line positions on the cartesian bite and twist angle, respectively, for representative values of the remaining parameters. We note firstly that the functional variation of the transition energies is virtually identical with respect to these two angles. This makes it all but impossible to retrieve both angles from spectroscopic data.

On the other hand, given the geometry, the model makes some rather definite predictions, qualitatively and quantitatively, about the splittings that should be observed. With increasing bite angle, one component of the $^2T_{1g}$ set is expected to move towards the ^2E_g set, and the overall splitting should increase from about 600 cm^{-1} at $\alpha = 0$. This is reinforced by a

TABLE 7

Band positions for ^2E_g and $^2T_{1g}$ transitions in some chromium(III) complexes

$[Cr(gly)_3]$ [a]	$[Cr(IDA)_2]^-$ [b]	$[Cr(MIDA)_2]^-$ [c]	$[Cr(PDC)_2]^-$ [d]	$[Cr(cys)_2]^-$ [e]
14,485	13,190 (?)	13,402	12,735	12,585
14,579	13,355	13,832 (?)	12,910	13,078 (?)
14,842	14,300	14,611	13,060	13,916
15,350	15,165	~15,020	13,162	14,566
15,442	15,165	~15,350	13,285	15,314
trans-$[Cr(en)_2F_2]^+$ [f]	$[Cr(ox)_3]^{3-}$ [g]	$[Cr(en)_3]^{3+}$ [h]	$[Cr(en)_3]^{3+}$ [i]	$[Cr(en)_3]^{3+}$ [j]
13,098	14,451	14,883	14,881	
	14,470	14,901	14,900	14,930
14,866	15,210	15,431	15,423	15,420
15,058	15,384	15,444	15,441	
15,277	15,421	15,514	15,508	15,720
	20,522			
	20,688			
	20,702			

[a] Ref. 63, 12 K. [b] Ref. 71, sodium salt, 20 K. [c] Ref. 71, sodium salt, 21 K. [d] Ref. 71, sodium salt, 5 K. [e] Ref. 79, sodium salt, 12 K. [f] Ref. 77, perchlorate salt, 5 K. [g] Refs. 66,68, doped in $NaMgAl(ox)_3$, 77 K. [h] Ref. 60, chloride salt, 6 K. [i] Ref. 61, doped in $[Ir(en)_3]Cl_3$, 7 K. [j] Ref. 62, aqueous solution, room temperature.

positive twist angle and counteracted by a negative one. Kepert has presented a model for tris(bidentate) complexes based on a classical repulsion force law, which predicts a negative twist angle, increasing in magnitude with increasing bite angle [54,55]. For our purposes, his results can be stated roughly as

$$\beta = -0.04\alpha^2 - 0.40\alpha \tag{9}$$

Thus we would expect that only small departures from the octahedral(O^*) transition energies would obtain for most $Cr(A-A)_3$ complexes. The ethylenediamine bite angle is 3.7° [56–59], which should lead to a twist angle of about −2°. The actual cartesian twist angle in the chloride salt is, however, almost zero [59], so that Fig. 4 is an appropriate gauge of the splittings to be expected.

Experimentally, problems abound in the assignment of the bands in question, because of the very large number of vibronic lines in the area. Flint's assignments from low temperature absorption spectra [60] and Güdel's from low temperature circular dichroism [61] coincide. The overall splitting of just over 600 cm^{-1} and the near-degeneracy of the $^2T_{1g}$ components would be very appropriate if the geometry was nearly octahedral, or if a large negative twist angle was incurred. From Fig. 4, however, we expect

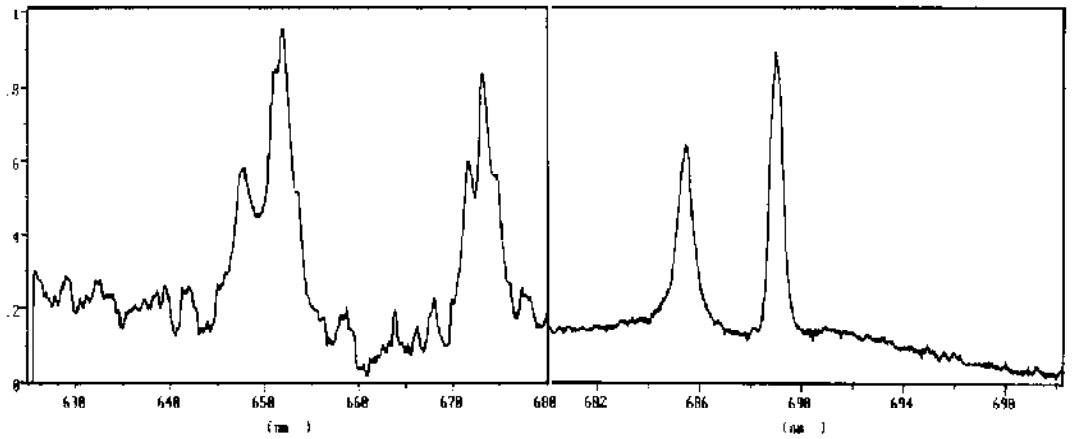

Fig. 8. A portion of the excitation spectrum of *fac*-[Cr(gly)$_3$] at 12 K. N_2 laser-pumped dye laser excitation: DCM in DMSO, 630–680 nm; Nile Blue in ethanol, 680–700 nm. Spectrum is corrected for laser intensity. Note abscissa scale change.

about 700 cm^{-1} of total splitting, with one $^2T_{1g}$ component moved approximately halfway toward the ^2E_g set. Of course, such a pattern is not difficult to find in the sharp line absorption and CD spectra, but it is interesting that Kaizaki has recently assigned (Table 7) the room temperature CD spectrum, based on an analysis of signs and magnitudes of rotatory strengths, in very good correspondence with the predictions of Fig. 4 [62].

Figure 8 shows the sharp line excitation spectrum [63] of the *facial* isomer of [Cr(gly)$_3$]. In the *facial* isomer the influence of the amino and carboxylate groups will tend to be averaged out, so that Fig. 4 is an approximate guide to the positions of the ^2E_g and $^2T_{1g}$ components. These five lines stand out well and demonstrate the 2-1-2 splitting pattern expected. From the X-ray crystal structure [64], $\alpha = 4.1°$ and β is small and positive (about 1°). Both the total splitting, and the position of the middle band would indicate an even larger value of α. This discrepancy, as well as the larger experimental ^2E_g splitting, is explained by the ligand field asymmetry (which is more important the greater the distortion from orthoaxiality) and the anisotropic π effects. Figure 9 is a plot of calculated transition energies as a function of $e_{\pi O}$ (anisotropic), using the atom positions from the X-ray crystal structure [64] and adjusting $e_{\sigma O}$ to keep the quartet energies approximately constant. The best fit, with no attempt at refinement of the other parameters, is near $e_{\pi O} = 1200$ cm^{-1}. It should be noted that for this and other complexes, room temperature crystal structures may not represent accurately the geometry at the temperature at which spectra were measured.

A third tris(bidentate) complex is $[Cr(ox)_3]^{3-}$. Experimental data for the $^2T_{2g}$ region [65,66] make this a useful example. The oxalate bite angle in the

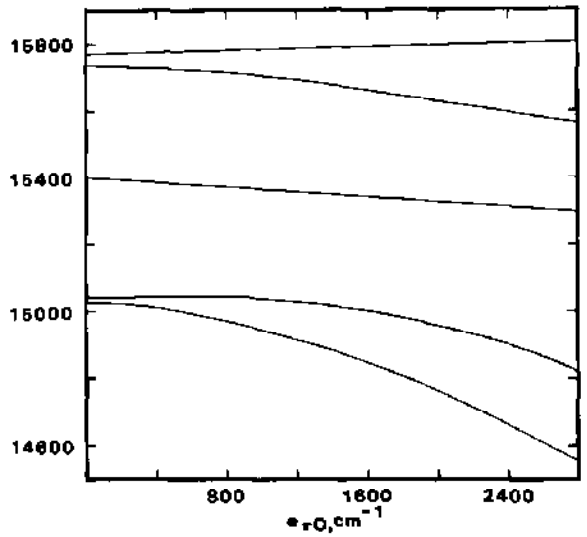

Fig. 9. Calculated (^2E_g, $^2T_{1g}$) transition energies for *fac*-[Cr(gly)$_3$] as a function of $e_{\pi O}$ (anisotropic). $e_{\sigma N} = 7000$, $e_{\sigma O} = \frac{1}{3}(19{,}500 - 2e_{\pi O})$.

potassium salt, 3.75° [67], is similar to that of ethylenediamine, but the twist angle is more negative than would be predicted from Kepert's model (about −5°). These are precisely the conditions under which the effects of the bite and twist distortions practically cancel, and at first glance the reported sharp line spectrum [66,68] matched Fig. 4 quite well near $\alpha = 0$.

The problem is that the anisotropic π effects from carboxylate coordination, which are certainly substantial, lead to quite different behavior from that depicted in Fig. 4. Figure 10 illustrates this behavior as a function of $e_{\pi O}$, with $e_{\sigma O}$ adjusted to $\frac{1}{3}(19{,}500 - 2e_{\pi O})$, which maintains roughly constant quartet positions, using the actual atom positions in $K_3[Cr(ox)_3]$ [67]. The $^2T_{1g}$ components are not greatly affected by the inclusion of π-anisotropy, and Coleman's assignments, from excitation spectra, can be accepted. But the ^2E_g components are calculated to show a remarkably large splitting. The best fit of the total (^2E_g, $^2T_{1g}$) splitting to Fig. 10 would place $e_{\pi O}$ near 1000 cm^{-1} with a ^2E_g splitting of about 200 cm^{-1}. The total (^2E_g, $^2T_{1g}$) splitting is, however, somewhat sensitive to changes in the interelectronic repulsion parameters, which were set arbitrarily in Fig. 10. The $^2T_{1g}$ splitting is much less sensitive, and fitting the experimental splitting of 210 cm^{-1} [66] to Fig. 10 would yield an $e_{\pi O}$ of around 1800 cm^{-1}. In any case, the ^2E_g splitting is predicted to be considerably larger than previously supposed. A good candidate for the ^2E_g partner is a prominent band 401 cm^{-1} from the 0–0 line in absorption spectra [65,69]. This band has been considered to be vibronic in origin (there was certainly little reason to suspect it to be a ^2E_g component) [69,70], from the Cr–O

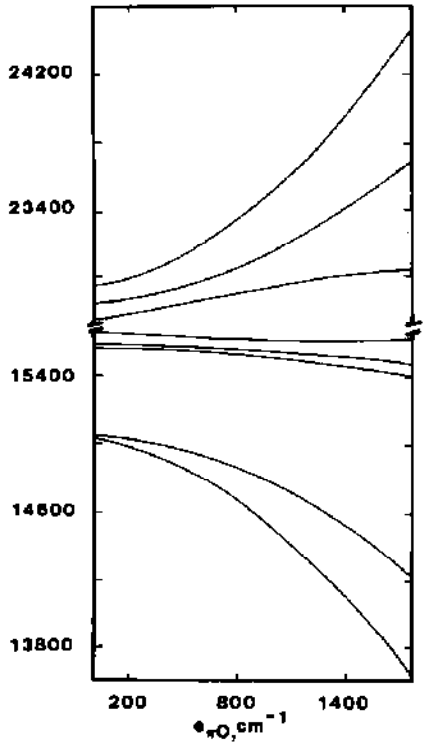

Fig. 10. Calculated (^2E_g, $^2T_{1g}$) transition energies for $K_3[Cr(ox)_3]$ as a function of $e_{\pi O}$ (anisotropic). $e_{\sigma O} = \frac{1}{3}(19{,}500 - 2e_{\pi O})$.

stretching mode, which is found at 416 cm^{-1} in infrared spectra [70] and in luminescence [69]. The luminescence peak is, however, quite weak, so that it is reasonable to suggest that the strong 401 cm^{-1} line in absorption is not the corresponding vibronic peak.

A very great variability in the ^2E_g splittings (from 2 to 115 cm^{-1}, as assigned [68]) of $[Cr(ox)_3]^{3-}$ in different crystals has been noted. In our view, these are not ^2E_g splittings at all, but are more likely to be due to inequivalent sites or close vibronic structure.

The $^2T_{2g}$ components have been assigned in close proximity [66], again as befits a nearly octahedral complex, while Fig. 10 points to a total splitting of about 1000 cm^{-1} (at $e_{\pi O} = 1400$ cm^{-1}). The sharp line absorption spectrum in the $^2T_{2g}$ region [65] encompasses over 1200 cm^{-1}, so that an assignment in concordance with Fig. 10 is quite possible.

The remaining complexes have approximate tetragonal symmetry. Table 7 presents Flint's data [71] for *cis*-$[Cr(IDA)_2]$, which are noteworthy for the large (2000 cm^{-1}) overall splitting of the (^2E_g, $^2T_{1g}$) set, but also in that the four bands listed are the only ones which stand out as electronic lines. Flint has attributed the two low energy bands to absorption and emission from

non-equivalent sites. Thus at most three lines can be associated with a single chromophore. These three are quite prominent, however, and the two higher energy lines (14,300 and 15,165 cm^{-1}) are unusually broad, so that one or more near-degeneracies may be involved.

Looking again at Fig. 2 (demonstrating anisotropic π effects), there are two places where a reasonably good fit to these data might be found. At $e_{\pi O} = 2000$ cm^{-1} the two states near 15,000 cm^{-1} in the Figure could appear as one band (the observed widths are over 200 cm^{-1} [71]). These and the lower two states then fit the experimental data quite well. This assignment would require the existence of another line near 15,700 cm^{-1} in the experimental spectrum. There is a peak in that location [71], but 2000 cm^{-1} is rather a large value for $e_{\pi O}$, judging by the previous discussion on $[Cr(gly)_3]$ and $[Cr(ox)_3]^{3-}$. A value of 1400 cm^{-1}, more consistent with the other carboxylates, is still consonant with the experimental data, but there would need to be a line near 13,900 cm^{-1} which is not identifiable in the experimental spectrum.

Flint also suspected another component in this region [71]. With either of the above assignments, his conclusion that only one electronic line was being observed near 13,000 cm^{-1} is supported by the calculations. It has been reasoned [71–73], using the approximation of D_{4h} holohedrized symmetry, that the $^2E_g(D_{4h})$ component of the $^2T_{1g}(O_h)$ state had dropped to become the lowest excited state. Figure 2 shows graphically the extent of mixing of the five doublet excited states at higher values of $e_{\pi O}$, and an eigenfunction analysis confirms this. The deviations from orthoaxiality and the π-anisotropy make the D_{4h} approximation a poor one.

$[Cr(MIDA)_2]^-$, H_2MIDA = methyliminodiacetic acid, has a *trans* rather than a *cis* configuration [74]. Its low temperature absorption spectrum has been measured but, aside from the luminescent origin, not assigned [71]. The energies listed in Table 7 represent a choice of the most prominent peaks in the spectrum. They are thus by no means certain, but Fig. 11, which makes use of atom coordinates from $K[Cr(i\text{-}PIDA)_2]$, the isopropyl analog [75], does line up reasonably well with these values at $e_{\pi O}$ between 1200 and 1400 cm^{-1}.

Unlike the IDA ligands, pyridinedicarboxylate, PDC^{2-}, coordinates meridionally [76]. An approximate geometric model would place the pyridine nitrogen exactly on the z axis, with the carboxylate oxygens in the xz or yz plane, displaced from the x or y axis by the cartesian bite angle, α. In Fig. 12 the π orbitals of both carboxylates and the pyridine nitrogen are chosen perpendicular to the ligand plane.

The low temperature absorption spectrum has been measured, and assigned by Flint [71] as shown in Table 7. Because Dq of pyridine and carboxylate are quite similar, the small (550 cm^{-1}) total splitting of the

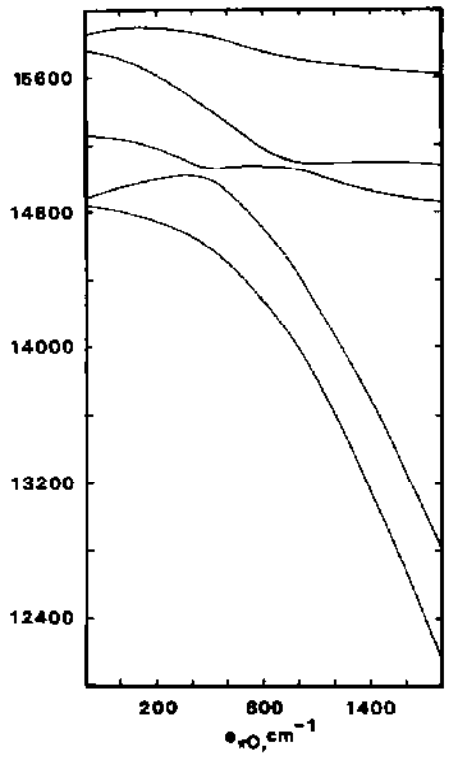

Fig. 11. Calculated (^2E_g, $^2T_{1g}$) transition energies for a *trans*-[Cr(MIDA)$_2$]$^-$ complex, using atom positions from the *N*-isopropyl analog, as a function of $e_{\pi O}$ (anisotropic). $e_{\sigma N} = 7000$, $e_{\sigma O} = \frac{1}{3}(19{,}500 - 2e_{\pi O})$.

(^2E_g, $^2T_{1g}$) components was deemed consistent. However, the ligand field asymmetry between two ligands is a two-dimensional one, and the *Dq* dimension is relatively unimportant with respect to the sharp line splitting in comparison with the orthogonal component [3]. Differences in e_π and in π-orientation are the most important factors, as is seen in several figures presented here. This is quite reasonable in view of the fact that all the Cr(III) sharp line transitions are within the t_{2g} subshell.

Lacking an X-ray crystal structure, and having to supply guesses for the angular overlap parameters, Fig. 12 is a crude representation of the relative doublet energies, but the conclusion nevertheless stands: the electronic lines should be found considerably further spread out, on the order of 2000 cm^{-1} or more.

trans-[Cr(en)$_2$F$_2$]$^+$ is another complex whose sharp line spectrum has been explained in terms of a crossover of the $^2E_g(D_{4h})$ to become the luminescent state [77]. As assigned the electronic lines span 2200 cm^{-1}, with one line missing from Table 7, the presumed $^2E_g(D_{4h})$ partner. Figure 13 constructs the (^2E_g, $^2T_{1g}$) energy levels, assuming for the ethylenediamines a cartesian

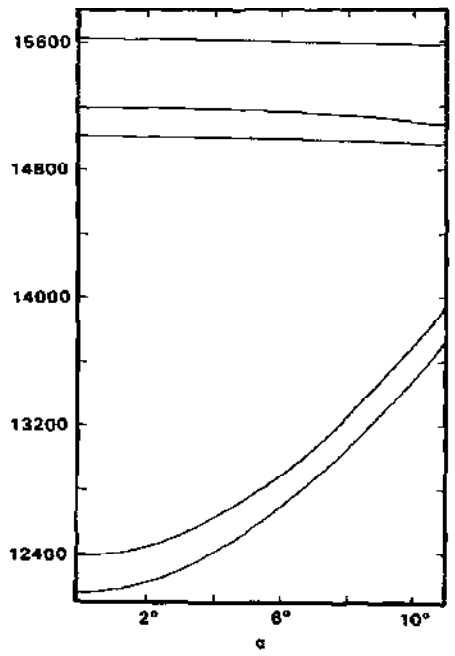

Fig. 12. Calculated (^2E_g, $^2T_{1g}$) transition energies for a $[Cr(PDC)_2]^-$ complex as a function of the cartesian bite angle α, assuming ligand orientations as described in text. $e_{\sigma N} = 7033$, $e_{\pi N} = 800$ (anisotropic), $e_{\sigma O} = 8367$, $e_{\pi O} = 1800$ (anisotropic).

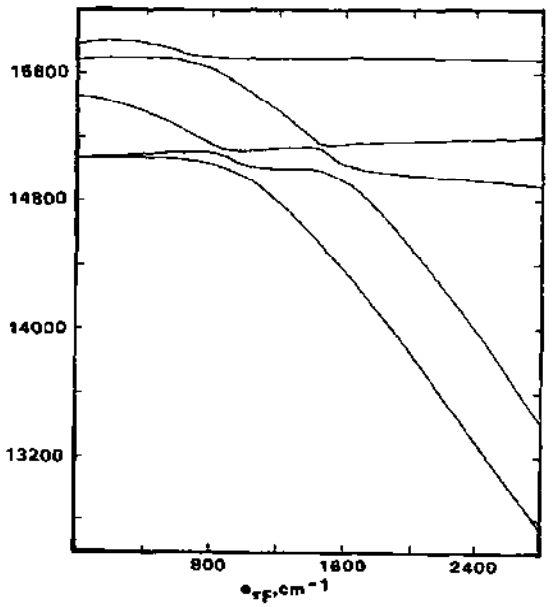

Fig. 13. Calculated (^2E_g, $^2T_{1g}$) transition energies for a *trans*-$[Cr(en)_2F_2]^+$ complex as a function of $e_{\pi F}$ (isotropic). M(N–N) distortion angles were assumed to be $\alpha = 3°$, $\beta = 0$. $e_{\sigma N} = 7000$, $e_{\sigma F} = \frac{1}{3}(19{,}000 - 4e_{\pi F})$.

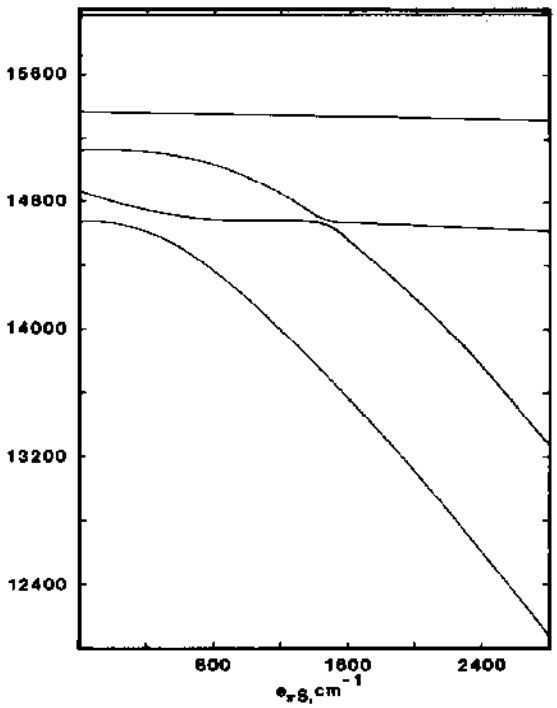

Fig. 14. Calculated (^2E_g, $^2T_{1g}$) transition energies for *trans*(*S*)-Na[Cr(cys)$_2$] as a function of $e_{\pi S}$ (anisotropic). $e_{\sigma N} = 7000$, $e_{\sigma O} = 7700$, $e_{\pi O}800$ (anisotropic), $e_{\sigma S} = \frac{1}{3}(18{,}000 - 2e_{\pi S})$.

bite angle of 3° and no twist, as a function of $e_{\pi F}$ (isotropic), again adjusting $e_{\sigma F}$ to maintain the quartet positions. The spectrum is best fit for $e_{\pi F}$ somehwere between 2000 and 2500 cm^{-1}. The missing line should be found some 700 cm^{-1} above the origin.

Na[Cr(cys)$_2$], H_2cys = cysteine, exhibits *facial* coordination with the sulfurs *trans* to each other [78]. A C_2 axis exists, so that four independent angles are necessary to specify the total angular geometry. The molecule is too complicated to retrieve much information from the spectrum, but a taste of the sharp line structure, plotting transition energies as a function of $e_{\pi S}$, can be seen in Fig. 14, using the geometry from the room temperature crystal structure, anisotropic π-bonding by sulfur and oxygen, and reasonable values for the other parameters. The 12 K sharp line excitation spectrum has been measured and extends over more than 3000 cm^{-1} in the (^2E_g, $^2T_{1g}$) region [79]. The data in Table 7 represent only the most prominent peaks. No assignment was made originally [79], and some of the peaks listed in Table 7 are possibly vibronic.

E. CONCLUSIONS

The main conclusion is that sharp line electronic data, when they can be obtained, can be quite useful. Sharp line splittings are much more sensitive

to the ligand field properties of the coordinating groups and to the coordination geometry than are broad band splittings. Some specific conclusions relating to sharp line spectra can be advanced:

1. Angular geometry must be included in the analysis. The model presented here is far from perfect, but the calculations are in much better agreement with experimental data when the angular geometry from a crystal structure is incorporated, or even if the geometry is only approximated, than if orthoaxiality is assumed.

2. An anisotropic π-interaction must be applied in treating non-linear ligators. Even approximating the orientation of the π orbitals will yield better results than ignoring this factor.

3. In some cases the effects of small changes in angular variables are sufficiently unique for it to be feasible to determine them from the spectrum.

4. In non-O_h complexes, spin–orbit coupling effects are swamped by others. There is little possibility of fixing ζ by spectral fitting.

5. Asymmetry in e_π is the most important ligand field contribution to the splitting of intraconfigurational transitions.

6. In many cases it is in principle possible to determine all angular overlap parameters, without the necessity of choosing one arbitrarily.

ACKNOWLEDGEMENT

Acknowledgement is made to the donors of The Petroleum Research Fund, administered by the ACS, for support of this research.

REFERENCES

1 A.B.P. Lever, Inorganic Electronic Spectroscopy, Elsevier, Amsterdam, 2nd edn., 1984.
2 F.S. Ham, Jahn–Teller Effects in Electron Paramagnetic Resonance Spectra. Plenum Press, New York, 1971.
3 P.E. Hoggard, Z. Naturforsch., Teil A, 36 (1981) 1276.
4 C.K. Jørgensen, Adv. Chem. Phys., 5 (1963) 33.
5 L.E. Orgel, J. Chem. Phys., 23 (1955) 1819.
6 H.L. Schläfer, H. Wagener, F. Wasgestian, G. Herzog and A. Ludi, Ber. Bunsenges. Phys. Chem., 75 (1971) 879.
7 C.D. Flint and P. Greenough, J. Chem. Soc. Faraday Trans. 2, 68 (1972) 897.
8 C.D. Flint, P. Greenough and A.P. Matthews, J. Chem. Soc. Faraday Trans. 2, 69 (1973) 23.
9 C.D. Flint and P. Greenough, J. Chem. Soc. Faraday Trans. 2, 70 (1974) 815.
10 C.D. Flint and D.J.D. Palacio, J. Chem. Soc. Faraday Trans. 2, 73 (1977) 649.
11 R.K. Mukherjee, S.C. Bera, and A. Bose, J. Chem. Phys., 56 (1972) 3720.
12 R.A. Condrate and L.S. Forster, J. Chem. Phys., 48 (1968) 1514.
13 W.N. Shepard and L.S. Forster, Theor. Chim. Acta, 20 (1971) 135.
14 C.D. Flint and A.P. Matthews, J. Chem. Soc. Faraday Trans. 2, 69 (1973) 419.

15 J. Hanuza, W. Strek, K. Hermanowicz, B. Jezowska-Trzebiatowska, and I. Trabjerg, Chem. Phys., 86 (1984) 137.
16 J.S. Griffith, The Irreducible Tensor Method for Molecular Symmetry Groups, Prentice-Hall, Englewood Cliffs, NJ, 1962.
17 J.S. Griffith, The Theory of Transition-Metal Ions, Cambridge University Press, 1961, Chapter 9.
18 J.C. Slater, Quantum Theory of Atomic Structure, Vols I and II, McGraw-Hill, New York, 1960.
19 C.E. Schäffer, Struct. Bonding, 14 (1973) 69.
20 H.-H. Schmidtke, Z. Naturforsch., Teil A, 19 (1964) 1502.
21 E.P. Wigner, Group Theory and its Application to the Quantum Mechanics of Atomic Spectra (English translation), Academic Press, New York, 1959, p. 167.
22 C.E. Schäffer, Struct. Bonding, 5 (1968) 68.
23 C.E. Schäffer and C.K. Jørgensen, Mol. Phys., 9 (1965) 401.
24 B.T. Smith, J.M. Boyle, J.J. Dongarra, B.S. Garbow, Y. Ikebe, V.C. Klema, and C.B. Moler, Matrix Eigensystem Routines—EISPACK Guide, Springer-Verlag, Berlin, 1976.
25 M.J.D. Powell, Comput. J., 7 (1964) 155.
26 J.L. Kuester and J.H. Mize, Optimization Techniques with Fortran, McGraw-Hill, New York, 1973.
27 A.A. Clifford, Multivariate Error Analysis, Wiley-Halstad Press, New York, 1973.
28 R.E. Trees, Phys. Rev., 83 (1951) 756.
29 G. Racah, Phys. Rev., 85 (1952) 381.
30 C.J. Ballhausen, Introduction to Ligand Field Theory, McGraw-Hill, New York, 1962.
31 J. Ferguson, Progr. Inorg. Chem., 12 (1970) 159.
32 J. Ferguson and D.L. Wood, Aust. J. Chem., 23 (1970) 861.
33 M. Gerloch and R.C. Slade, Ligand-Field Parameters, Cambridge University Press, 1973.
34 C.K. Jørgensen, Modern Aspects of Ligand Field Theory, North-Holland, Amsterdam, 1971.
35 C.D. Flint, A.P. Matthews, and P.J. O'Grady, J. Chem. Soc. Faraday Trans. 2, 73 (1977) 655.
36 P.E. Noorman and J. Schrijver, Physica, 36 (1967) 547.
37 C.K. Jørgensen, Progr. Inorg. Chem., 4 (1962) 73.
38 P.E. Hoggard, Z. Naturforsch. Teil A, 37 (1982) 1096.
39 D. Mootz and H. Wunderlich, Acta Cyrstallogr., Sect. B, 36 (1980) 445.
40 C.E. Schäffer, Proc. R. Soc. (London), Ser. A, 297 (1967) 96.
41 B.M. Foxman, Inorg. Chem., 17 (1978) 1932.
42 J.C. Eisenstein, J. Chem. Phys., 34 (1961) 1628.
43 W.A. Runciman and K.A. Schroeder, Proc. R. Soc. (London), Ser. A, 265 (1962) 489.
44 A.D. Liehr, J. Phys. Chem., 67 (1963) 1314.
45 J.P. Jesson, J. Chem. Phys., 48 (1968) 161.
46 E. König and S. Kremer, Ligand Field Energy Diagrams, Plenum Press, New York, 1977.
47 R.K. Mukherjee, S.C. Berà, and A. Bose, J. Chem. Phys., 53 (1970) 1287.
48 J.J. Alexander and H.B. Gray, J. Am. Chem. Soc., 90 (1968) 4260.
49 J.A. LoMenzo, S. Strobridge, H.H. Patterson, and H. Engstrom, J. Mol. Spectrosc., 66 (1977) 150.
50 C.K. Jørgensen and K. Schwochau, Z. Naturforsch. Teil A, 20 (1965) 65.
51 C.D. Flint and A.G. Paulusz, Mol. Phys., 44 (1981) 925.
52 J.C.D. Brand, G.L. Goodman and B. Weinstock, J. Mol. Spectrosc., 38 (1971) 464.
53 C.D. Flint and A.P. Matthews, J. Chem. Soc. Faraday Trans. 2, 70 (1974) 1301.

54 D.L. Kepert, Progr. Inorg. Chem., 23 (1979) 1.
55 D.L. Kepert, Inorganic Stereochemistry, Springer-Verlag, Berlin, 1982.
56 A. Whuler, C. Brouty, P. Spinat, and P. Herpin, Acta Crystallogr., Sect. B, 34 (1978) 793.
57 C. Brouty, P. Spinat, A. Whuler, and P. Herpin, Acta Crystallogr., Sect. B, 33 (1977) 1913.
58 N.W. Alcock, P. deMeester, and T.J. Kemp, Acta Cyrstallogr., Sect. B, 34 (1978) 3367.
59 A. Whuler, C. Brouty, P. Spinat, and P. Herpin, Acta Crystallogr., Sect. B, 31 (1975) 2069.
60 C.D. Flint and A.P. Matthews, J. Chem. Soc. Faraday Trans. 2, 72 (1976) 579.
61 U. Geiser and H.U. Güdel, Inorg. Chem., 20 (1981) 3013.
62 S. Kaizaki, M. Ito, N. Nishimura, and Y. Matsushita, Inorg. Chem., 24 (1985) 2080.
63 W.M. Wallace and P.E. Hoggard, Inorg. Chem., 22 (1983) 491.
64 R.F. Bryan, P.T. Greene, P.F. Stokely and E.W. Wilson, Jr., Inorg. Chem., 10 (1971) 1468.
65 O.S. Mortensen, J. Chem. Phys., 47 (1967) 4215.
66 W.F. Coleman, J. Lumin., 22 (1980) 17.
67 D. Taylor, Aust. J. Chem., 31 (1978) 1455.
68 W.F. Coleman, J. Lumin., 10 (1975) 163.
69 R.A. Condrate and L.S. Forster, J. Mol. Spectrosc., 24 (1967) 490.
70 P.E. Hoggard and H.-H. Schmidtke, Spectrochim. Acta, Part A, 31 (1975) 1389.
71 C.D. Flint and A.P. Matthews, J. Chem. Soc. Faraday Trans. 2, 71 (1975) 379.
72 P.E. Hoggard and H.-H. Schmidtke, Ber. Bunsenges. Phys. Chem., 76 (1972) 1013.
73 H.-H. Schmidtke and P.E. Hoggard, Chem. Phys. Lett., 20 (1973) 119.
74 J.A. Weyh and R.E. Hamm, Inorg. Chem., 7 (1968) 2431.
75 D. Mootz and H. Wunderlich, Acta Crystallogr., Sect. B, 36 (1980) 721.
76 P.E. Hoggard and H.-H. Schmidtke, Inorg. Chem., 12 (1973) 1986.
77 C.D. Flint and A.P. Matthews, J. Chem. Soc. Faraday Trans. 2, 70 (1974) 1307.
78 P. deMeester, D.J. Hodgson, H.C. Freeman and C.J. Moore, Inorg. Chem., 16 (1977) 1494.
79 W.M. Wallace, Ph.D. Dissertation, Polytechnic Institute of New York, 1982.